European Journal of Cell Biology 103 (2024) 151373

Contents lists available at ScienceDirect

European Journal of Cell Biology

journal homepage: www.elsevier.com/locate/ejcb

Impact of heat and cold shock on epigenetics and chromatin structure

Claudio Casali [a,*], Luca Galgano [b], Lorena Zannino [a], Stella Siciliani [a], Margherita Cavallo [a], Giuliano Mazzini [c], Marco Biggiogera [a]

[a] Laboratory of Cell Biology and Neurobiology, Department of Biology and Biotechnology "L. Spallanzani", University of Pavia, 27100 Pavia, Italy
[b] Laboratory of Biochemistry, Department of Biology and Biotechnology "L. Spallanzani", University of Pavia, 27100 Pavia, Italy
[c] Institute of Molecular Genetics IGM-CNR, 27100 Pavia, Italy

ARTICLE INFO

Keywords:
Heat shock
Cold shock
Epigenetics
Methylation
Histone post translational modifications
Chromatin condensation

ABSTRACT

Cells are continuously exposed to various sources of insults, among which temperature variations are extremely common. Epigenetic mechanisms, critical players in gene expression regulation, undergo alterations due to these stressors, potentially leading to health issues. Despite the significance of DNA methylation and histone modifications in gene expression regulation, their changes following heat and cold shock in human cells remain poorly understood. In this study, we investigated the epigenetic profiles of human cells subjected to hyperthermia and hypothermia, revealing significant variations. Heat shock primarily led to DNA methylation increments and epigenetic modifications associated with gene expression silencing. In contrast, cold shock presented a complex scenario, with both methylation and demethylation levels increasing, indicating different epigenetic responses to the opposite thermal stresses. These temperature-induced alterations in the epigenome, particularly their impact on chromatin structural organization, represent an understudied area that could offer important insights into genome function and potential prospects for therapeutic targets.

1. Introduction

The field of epigenetics has witnessed rapid growth over the last few decades, revolutionizing the current understanding of genetics. Epigenetic modifications are fundamental mechanisms for controlling gene expression, and their dysregulation is central to the development of various pathologies, including neurodegenerative disorders and cancer (Huang and Figueroa, 2021; Livernois et al., 2021; Sharma and Tollefsbol, 2022). Epigenetic processes play central roles in driving the compaction and decompaction of DNA molecules, resulting in dynamic gene expression conditions (Cavalli and Heard, 2019; Xie and Liu, 2021). Various modifications, such as DNA methylation, covalent histone tails modifications, presence of histone variants, and RNA modifications, determine unique chromatin states (Binder et al., 2022). The occurrence of these chemical tags can be influenced by the effects of environmental factors or by internal homeostasis (Tyagi et al., 2021).

In eukaryotes, 5-methylcytosine (5mC) is the most prevalent form of DNA methylation, catalysed by a family of enzymes called DNA methyltransferases (DNMTs) (Li et al., 2022). These enzymes are responsible for the covalent transfer of a methyl group (CH_3) to the fifth position of a cytosine (C) pyrimidine ring, thus forming 5-methylcytosine. Since its discovery, the most common interpretations associate 5mC with transcriptional inhibition, either by determining compact genome organization or by sterically hinder the accessibility of the transcriptional machinery (Greenberg and Bourc'his, 2019; Santiago et al., 2020; Lam and Chen, 2022). Traditionally considered irreversible due to the resilience of carbon-carbon bonds, several studies have recently shown that DNA methylation is rather a dynamic process (Turpin and Salbert, 2022). The ten-eleven translocation (TET) family are Fe(II)- and α-ketoglutarate-dependent dioxygenases that catalyze iterative oxidation of 5mC to 5-hydroxymethylcytosine (5hmC), 5-formylcytosine (5fC) and 5-carboxylcytosine (5caC), ultimately leading to DNA demethylation (Wang et al., 2022; Joshi et al., 2022). 5hmC is the initial and most stable intermediate of 5mC oxidation, and it has been suggested to function as an independent epigenetic mark. Indeed, studies on 5hmC genomic distribution have revealed its preferential enrichment in the bodies of transcriptionally active genes, promoters, and enhancers (He et al., 2021).

Histone post-translational modifications (PTMs) also hold a dynamic regulatory potential, as the configuration of the modified residues is recognized by structural motifs within chromatin-modulating complexes (Li and Li, 2021; Casali et al., 2022b). For instance, histone

* Corresponding author.
E-mail address: claudio.casali@unipv.it (C. Casali).

https://doi.org/10.1016/j.ejcb.2023.151373
Received 21 September 2023; Received in revised form 1 November 2023; Accepted 14 November 2023
Available online 23 November 2023

Table 1
List of antibodies used for EM immunolabelling. Antibodies name, host, target, dilution, and RRID are reported.

Antibody (Host)	Target	Dilution	Reference (RRID)
Anti-5mC (mouse)	5mC	1 : 500 in PBS/BSA/TWEEN20	GTX629448 - AB_2888114 (GeneTex)
Anti-5hmC (mouse)	5hmC	1 : 150 in PBS/BSA/TWEEN20	GTX629765 - AB_2736902 (GeneTex)
Anti-DNMT3a (rabbit)	DNMT3a	1 : 10 in PBS/BSA/TWEEN20	GTX129125 - AB_2885902 (GeneTex)
Anti-TET2 (mouse)	TET2	1 : 20 in PBS/BSA/TWEEN20	GTX629881 - AB_2888171 (GeneTex)
Anti-H3K9me3 (rabbit)	H3K9me3	1 : 20 in PBS/BSA/TWEEN20	GTX121677 - AB_10721938 (GeneTex)
Anti-H3K9Ac (rabbit)	H3K9Ac	1 : 20 in PBS/BSA/TWEEN20	GTX88007 - AB_10731164 (GeneTex)
Anti-H3K27me3 (rabbit)	H3K27me3	1 : 20 in PBS/BSA/TWEEN20	GTX121184 - AB_10618572 (GeneTex)
Anti-Rabbit 12 nm gold particle conjugated (goat)	Rabbit IgG	1 : 20 in PBS	111–205–144 - AB_2338016 (Jackson ImmunoResearch)
Anti-Mouse 12 nm gold particle conjugated (goat)	Mouse IgG	1 : 20 in PBS	115–205–068 - AB_2338730 (Jackson ImmunoResearch)

Table 2
List of antibodies used for fluorescence immunolabelling. Antibodies name, host, target, dilution, and RRID are reported.

Antibody (Host)	Target	Dilution	Reference (RRID)
Anti-EZH2 (rabbit)	EZH2	1 : 200 in PBS/BSA1%	GTX110384 - AB_2885283 (GeneTex)
Alexa 568 (goat)	Rabbit IgG	1 : 100 in PBS/BSA1%	A11036 - AB_10563566 (Invitrogen)

Table 3
List of oligonucleotide primers used for gene expression analysis.

Target Gene	Sequence
EZH2 forward sequence (5' to 3')	GCGGATAAAGACCCCACCAA
EZH2 reverse sequence (5' to 3')	GCTGGGCCTGCTACTGTTAT
RPS18 forward sequence (5' to 3')	ATTAAGGGTGTGGGCCGAAG
RPS18 reverse sequence (5' to 3')	AAGTGACGCAGCCCTCTATG
GADPH forward sequence (5' to 3')	CCACAGTCCATGCCATCACT
GADPH reverse sequence (5' to 3')	GCCTGCTTCACCACCTTCTT

acetylation, involving the transfer of an acetyl group from acetyl-CoA to a lysine residue on the target histone tail, results in the removal of a positive charge on the histone. This weakens its interaction with DNA, hence reducing chromatin compaction and increasing accessibility to the transcriptional machinery (Aricthota et al., 2022). In contrast, histone methylation does not directly affect the electrostatic bond, but indirectly influences the recruitment and binding of multiple regulatory proteins. Consequently, histone methylation can lead to either transcriptional repression or activation, depending on the modified amino acid residue (Collins et al., 2019). Notably, among the histone methylating enzymes, the Polycomb group (PcG) proteins have drawn considerable attention for their crucial role in transcription repression through chromatin compaction (Parreno et al., 2022).

Temperature alterations are among the most common insults cell must deal with. Organisms need to rapidly respond to heat or cold stress, as maintenance of nuclear and genome integrity is of utmost importance (Azarm and Smith, 2020; Abildgaard et al., 2023). Moreover, with global temperature changes, the impact of thermal stress is expected to increase (Raftery et al., 2017). Adaptation to the environment has for long been uniquely attributed to mere genetic variations, however genetic regulation alone cannot fully explain the process of response to thermal stress, which is known to alter multiple biological functions and regulatory mechanisms. Phenotypic plasticity is crucial for cellular and organismal responses to environmental temperature changes, and epigenetic mechanisms have been recognized as the factors mediating adaptation, given their rapidity and dynamicity (Metzger and Schulte, 2017). Indeed, several studies have already highlighted the existence of a temperature-dependent epigenetic control of gene expression. However, to our knowledge, despite extensive descriptions of epigenetic changes following thermal stress in plants (Zhu et al., 2023) and animals (Wu et al., 2020), there is limited evidence regarding the effects on human cells. Expanding the current understanding of the effects of temperature variations on the human epigenome could hold a potential role to understand impacts on health (McCaw et al., 2020).

2. Materials and methods

2.1. Cell culture and treatments

HeLa cells were cultured in Dulbecco's modified Eagle medium (DMEM) supplemented with 10% fetal bovine serum (FBS) and 1% penicillin/streptomycin at 37 °C in a humidified atmosphere (95% air/5% CO_2). 48 h before experiments, cells were grown in 25 cm^2 flasks. At approximately 80% confluence, cells were subjected to thermal stress following heat and cold shock techniques described in (Liu et al., 1994; Yang et al., 2022). Heat shock was applied by exposing cells to 43 °C for 1 h and 30 min, followed by a recovery period at 37 °C for 1 h. Cold shock was induced by incubating cells at 4 °C for 6 h, followed by a recovery period at 37 °C for 2 h. For subsequent analyses, cells were either fixed or processed immediately after the shock (hyperthermia and hypothermia) or immediately after the recovery period following the shock (hyperthermia recovery and hypothermia recovery).

2.2. Transmission electron microscopy sample preparation

Cells were harvested by mild trypsinization with 0.25% trypsin in Phosphate Saline Buffer (PBS) containing 0.05% ethylene diamine tetraacetic acid (EDTA), centrifuged at 150 g for 10 min and then processed for either immunocytochemical or morphological analysis. For immunocytochemistry, cells were fixed with 4% paraformaldehyde (PFA) at room temperature (RT) for 30 min and then at 4 °C for 1 h and 30 min. After fixation, cells were rinsed with PBS, pre-embedded in 2% agarose, incubated in 0.5 M NH_4Cl at 4 °C for 30 min, dehydrated using graded ethanol, and finally embedded in acrylic resin (LR White, Agar Scientific, Stansted, UK). For morphological analysis, cells were fixed with 2.5% glutaraldehyde in culture medium for 2 h at RT. Following PBS rinses, cells were post-fixed using 1% aqueous OsO_4 for 2 h at RT, pre-embedded, dehydrated using graded acetone, and embedded in epoxy resin (EM-bed812, Electron Microscopy Sciences, Hatfield, PA, USA). Ultrathin sections (60–80 nm) were cut on a Reichert OM-U3 ultramicrotome and collected on nickel grids (200 Mesh). The specimens were observed with a JEM 1200 EX II electron microscope (JEOL, Peabody, MA, USA) operating at 100 kV and equipped with a MegaView G2 CCD camera (Olympus OSIS, Tokyo, Japan).

2.3. Transmission electron microscopy immunocytochemistry

Grids for immunocytochemical analyses were initially floated on a drop of normal goat serum (NGS) and subsequently incubated overnight (ON) at 4 °C in a drop of primary antibody (Table 1). Grids were then rinsed in PBS/TWEEN20 and PBS, floated on NGS and incubated with the appropriate colloidal gold-particle-conjugated secondary antibodies for 30 min at RT. Final rinses were performed in PBS and dH_2O. As negative controls, the same experimental procedures were performed

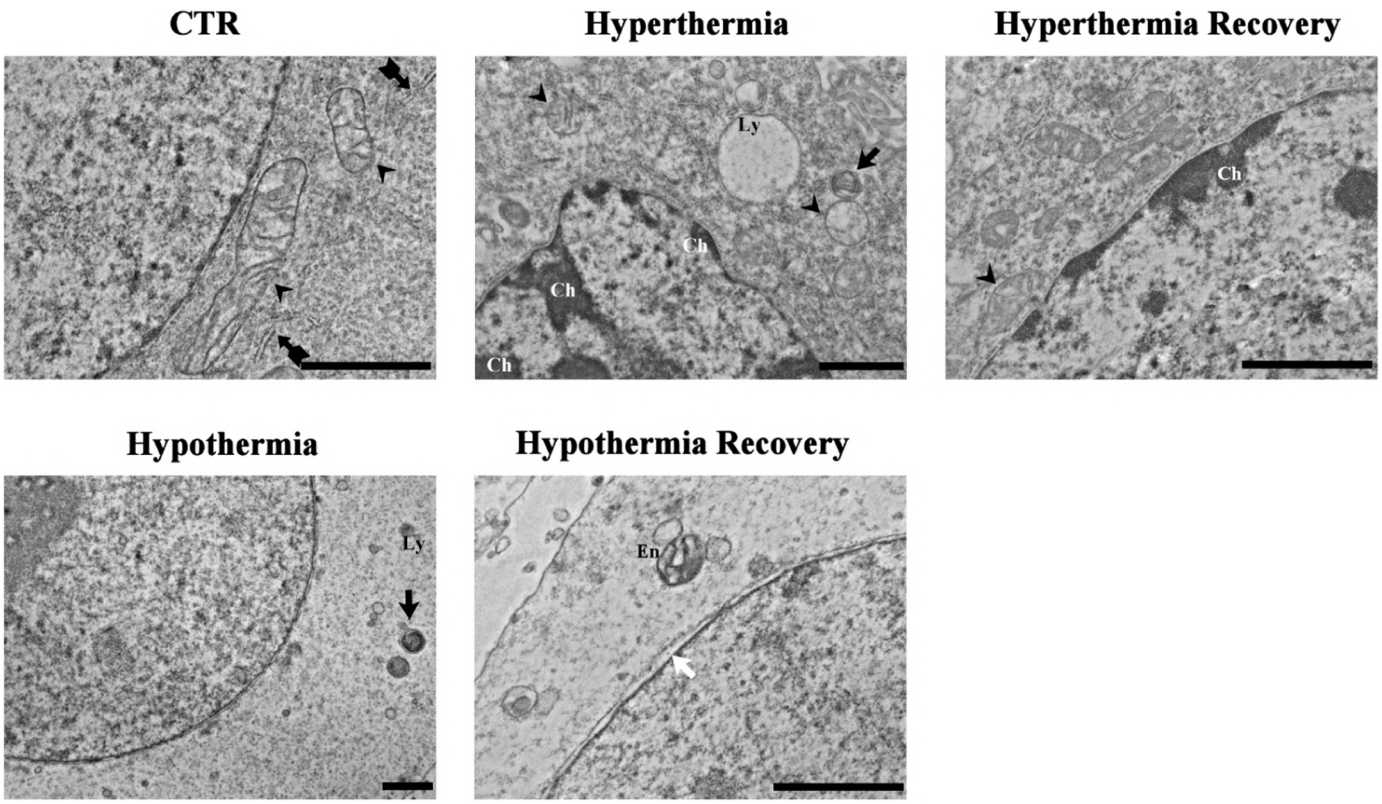

Fig. 1. Transmission electron microscopy morphological investigation. Control cells display normal morphological features, including well-defined organelles with intact structures (arrowhead: mitochondria; flagged arrow: rough endoplasmic reticulum). Following experimental stress, mitochondria frequently exhibited swelling or showed cristae damage, while MVBs are formed (dark arrow). Nuclear alterations included detachment of the two nuclear membranes (white arrow) and induction of chromatin clumps (Ch). Ly: lysosome; En: endosome. Bars: 1 μm.

using equal volumes without the primary antibody.

2.4. EDTA regressive technique and Reynolds' Lead Citrate Stain

Grids for immunocytochemistry were stained according to the EDTA regressive technique. Specifically, after pre-staining with 4% uranyl acetate, sections were incubated in 0.2 M EDTA at RT and subsequently post-stained with lead citrate (Bernhard, 1969). Staining for morphological analysis was performed according to the Reynolds' Lead Citrate Stain. Grids were floated on 4% uranyl acetate and then incubated in lead citrate (Reynolds, 1963).

2.5. Flow cytometry

Cells were detached by mild trypsinization, followed by centrifugation at 150 g for 10 min and subsequent suspension in fresh medium. A multiparametric analysis focusing on morphology and fluorescent labelling was conducted. Specifically, morphological analysis was based on the direct detection of both side scatter (SSC) and forward scatter (FSC) light. Subpopulations of cells were distinguished using a polygon-based method to identify areas corresponding to morphologically altered or unaltered cells (Buzzella et al., 2019). Cells staining was performed using propidium iodide (PI) at low concentration of 1 μg mL^{-1} for 15 min to label damaged cells (Mazzini and Danova, 2017). PI red fluorescence was detected with a 610 nm long-pass emission filter. Three independent measurements with a minimum of 50,000 cells per sample were performed. Samples were processed with a Partec CyFlow Space cytometer (Münster, Germany), equipped with argon laser excitation (power 200 mW) at 488 nm. Data were analyzed with the built-in software (Flowmax, Partec).

2.6. Confocal and STED microscopy sample preparation and immunocytochemistry

Cells were cultured on coverslips and fixed with 4% formalin for 20 min at RT. Cells were then post-fixed with 70% ethanol at − 20 °C for a minimum of 24 h. Samples were then rehydrated in PBS at RT and processed either for DNA staining or immunocytochemistry. For confocal microscopy, DNA was stained with SPY505-DNA (Spirochrome, Stein am Rhein, Switzerland). For immunocytochemistry, cells were incubated in PBS/BSA 3% for 20 min and then in the primary antibody (Table 2) for 1 h at RT. After rinsing in PBS, the samples were incubated with the appropriate secondary antibody for 45 min at RT. Following rinses, DNA was stained with SPY505-DNA. Coverslips were mounted using Mowiol and observed with a Leica TCS SP8 STED 3X, equipped with a 660 nm depletion laser (Wetzlar, Germany) to perform double STED.

2.7. SDS-PAGE and western blotting

Cells were harvested by mild trypsinization, centrifuged at 180 g for 10 min and rinsed twice in PBS. Subsequently, samples were incubated in Radioimmunoprecipitation assay (RIPA) lysis buffer 2X~~n~~with addition of protease and phosphatase inhibitors (aprotinin 100 μg/mL (Sigma-Aldrich), leupeptin 200 μg/mL (Sigma-Aldrich), PMSF 4 mM (Sigma-Aldrich), Na_3VO_4 4 mM (Sigma-Aldrich), NaF 4 mM (Sigma-Aldrich)). Protein quantification was performed using the Bicinchoninic acid (BCA) assay (Euroclone, Milano, Italy) and the absorbance was measured at a wavelength of 562 nm using a double beam spectrophotometer SHIMADZU UV-1601 (Kyoto, Japan). Samples were denatured using sodium dodecyl sulphate (SDS) 3X + 3% β-mercaptoethanol (Sigma-Aldrich) and separated by SDS-PAGE in a discontinuous system,

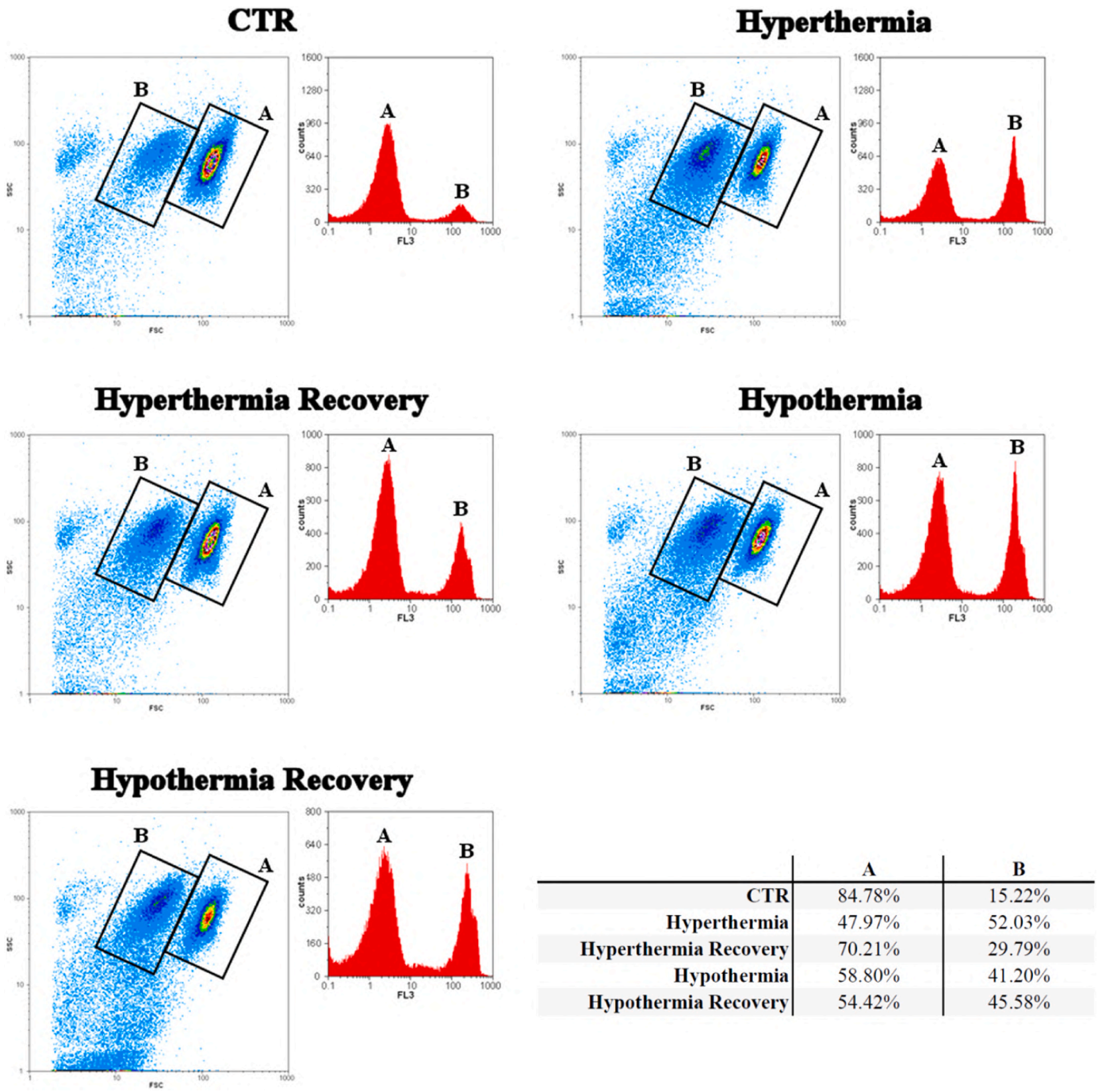

	A	B
CTR	84.78%	15.22%
Hyperthermia	47.97%	52.03%
Hyperthermia Recovery	70.21%	29.79%
Hypothermia	58.80%	41.20%
Hypothermia Recovery	54.42%	45.58%

Fig. 2. Representative flow cytometric analysis of cells in the different experimental conditions. Morphological patterns are assessed by means of SSC and FSC parameters, while PI positivity indicative of damaged cells is expressed by the fluorescent signal-to-cell counts ratio. A: intact cells; B: damaged cells.

consisting of a stacking gel (3%) and a running gel (6%, 10%, and 15%) based on protein molecular weight. Precision Plus Protein Standards All Blue (Bio-Rad, Hercules, CA, USA) were loaded as the molecular weight ladder. Electrophoresis was performed in a MINI-PROTEAN III electrophoretic chamber (Bio-Rad) applying a constant voltage of 150 V for 60 and 120 min. Proteins were then transferred from the gel onto a polyvinylidene difluoride (PVDF) membrane (Bio-Rad) using an electrophoretic chamber MINI-PROTEAN III (Bio-Rad) applying a constant electric current of 200 mA for 2 h. After 60 min incubation in a solution of 5% BSA in Tris-buffered saline (TBS), PVDF was incubated in primary antibodies (*see* Tables 1 and 2) diluted 1:1000 in 5% BSA in TBS, 0.02% NaN_3, 0.1% TWEEN20, ON at 4 °C. After rinses in washing buffer (PBS + 0.1% TWEEN20), PVDF was incubated with the appropriate horseradish-peroxidase-conjugated secondary antibody diluted 1:2000 (anti-rabbit) or 1:5000 (anti-mouse) in washing buffer for 60 min at RT. After rinses in washing buffer, proteins were visualized using an enhanced chemiluminescence (ECL) kit and the light emission was detected using a ChemiDoc XRS system (Bio-Rad).

2.8. Real time PCR (qPCR)

Cells were harvested by mild trypsinization and centrifuged at 150 g for 5 min. RNA extraction was performed using the RNeasy Kit (Qiagen, Hilden, Germany) and the samples were quantified using a Nanodrop 2000 Spectrophotometer (Thermo Fisher Scientific). mRNA was retrotranscribed using the Superscript IV protocol (Invitrogen), heating at

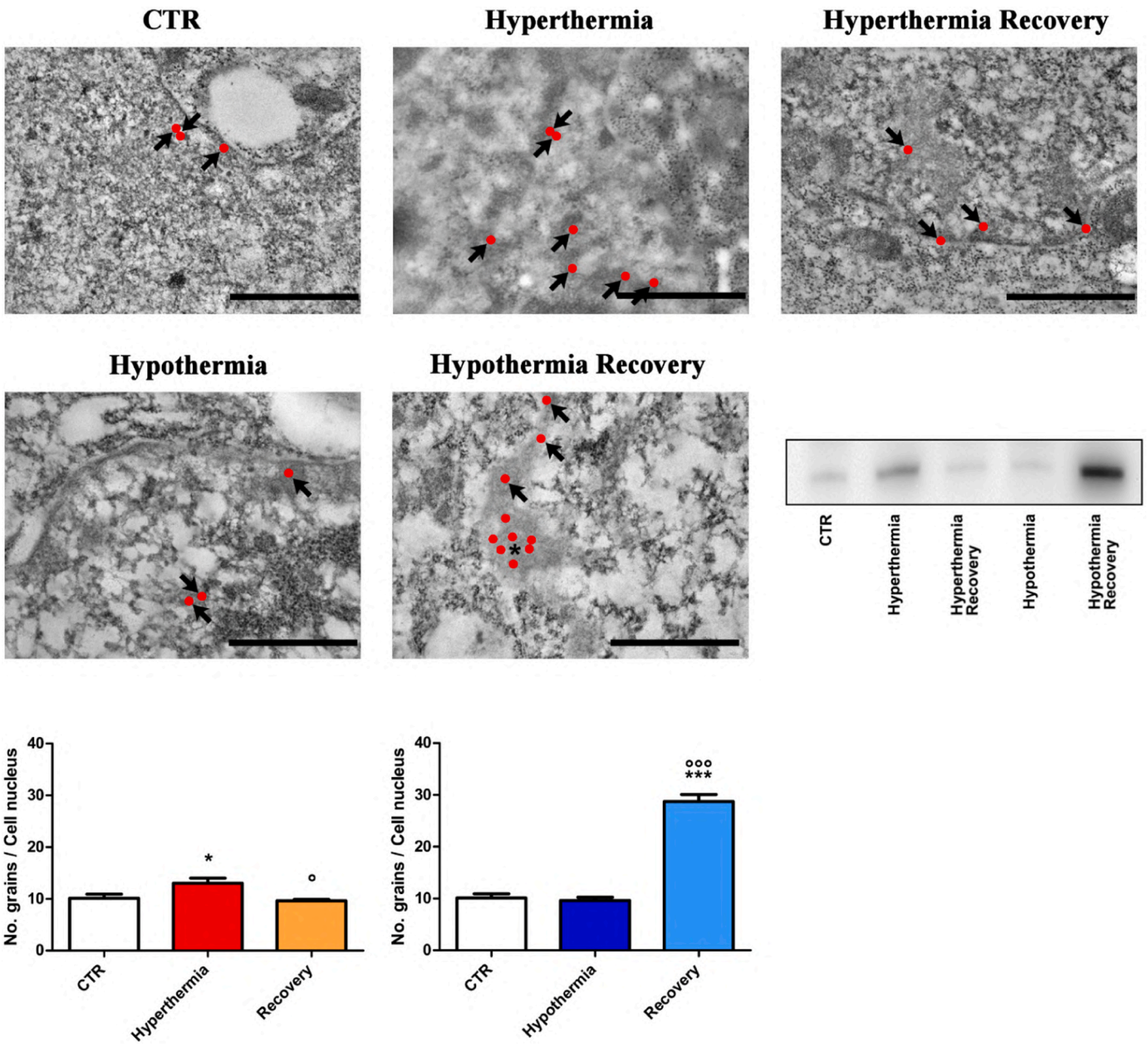

Fig. 3. H3K9me3 levels during thermal stresses. Immunolabelling (arrows) highlights significant increments in cells during hyperthermia and hypothermia. Data are supported by western blotting. Note the preferential localization of this marker in compacted chromatin region (asterisk). Bars: 500 nm.

65 °C for 5 min 50 ng/μL random examers, 10 mM dNTPs mix and template RNA in RNase-free water. After incubation on ice, the Superscript IV buffer, 100 mM dithiothreitol, ribonuclease inhibitor and the Superscript IV reverse transcriptase (200 U/μL) were added and the thermal cycler was run under the following parameters: 23 °C for 10 min, 55 °C for 10 min and 80 °C for 10 min. The analysis involved evaluating EZH2 expression using RPS18 and GADPH as reference genes. Primers were selected using the following Primer3 setup: 18–20–23 nucleotides length, 58–60–63 °C melting temperature with a maximum difference of 2 °C between forward and reverse primers, 100–300 product size range, resulting in a final 281 product size (Table 3). Data were analyzed using CFX Manager Software Version 1.5 (Bio-Rad).

2.9. Data and statistical analysis

Three independent replicates were performed for each experiment a statistical evaluation was conducted on. For EM immunolabelling, secondary antibody-conjugated colloidal gold grains were counted by three independent operators. Thirty nuclei displaying similar characteristics in term of size, nuclear envelope extension, and the ratio between heterochromatin and euchromatin were selected to ensure that any observed variances were not due to fundamental differences among cells. For confocal analysis, twenty nuclei were randomly chosen, and fluorescence intensity was assessed on three planes per cell. Data were presented as box plot with a range of 5–95 percentile. Fluorescence intensity in both confocal and STED analyses was normalized relative to the control. Statistical analysis was performed using one-way ANOVA with Bonferroni's post hoc test using GraphPad Prism version 5.03 (GraphPad Software, La Jolla, CA, USA). The mean values with standard error of the mean (SEM) are reported in the histograms. p-values from $p < 0.05$ were considered statistically significant (* indicates statistically relevant differences "vs CTR", ° indicates statistically relevant differences "vs stress conditions"; *:*p* Value <0.05; **:*p* Value < 0.01;

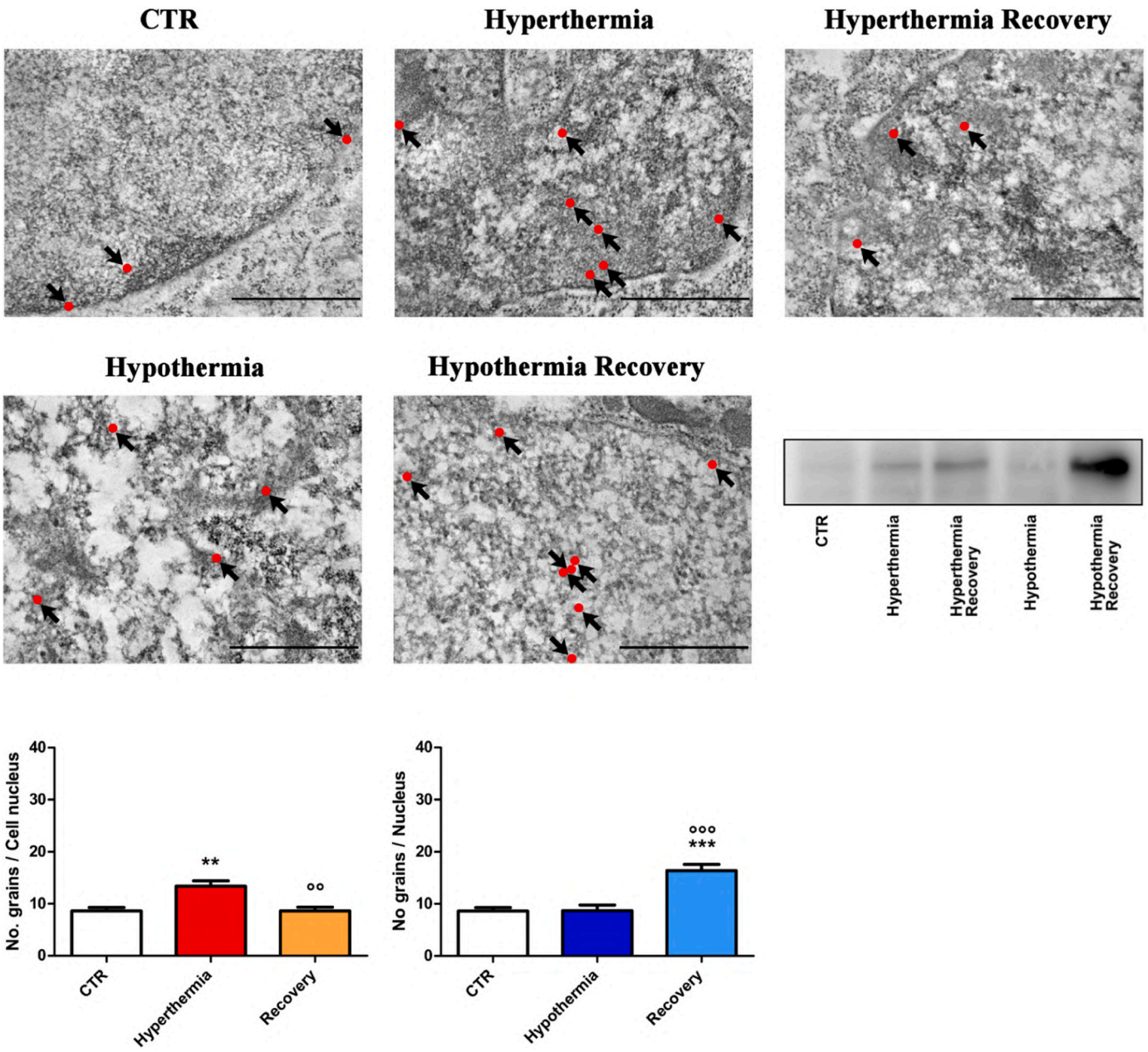

Fig. 4. H3K27me3 levels during thermal stresses. Immunolabelling (arrows) and western blot display relevant increase in H3K27me3 levels during heat shock and cold shock recovery. Note the histone location in heterochromatin and at its periphery. Bars: 500 nm.

***:p Value < 0.001). Images were processed using ImageJ2 and Fiji (Schindelin et al., 2012; Rueden et al., 2017), according to the standard of ethics in image processing. For TEM immunogold labelling, colloidal gold particles have been post-processed with false-colouring for readability. Deconvolution was performed using the Huygens Software (Scientific Volume Imaging, Hilversum, The Netherlands). Pearson coefficients were calculated using Fiji and the JaCoP plug-in on deconvolved STED images as described by (Hoboth et al., 2023). Tables were assembled using Jasc Paint Shop Pro version 7.02.

3. Results

3.1. Ultrastructural analysis reveals morphological alterations under experimental conditions

The ultrastructural analysis of cell morphology under the experimental conditions showed well-defined damage indicator. Assessment of the cytoplasm revealed the induction of multilamellar and multivesicular bodies (MVBs), which are clear examples of cell stress, along with abundant cytoplasmic vacuolization and lysosome presence. Additionally, mitochondria often appeared swollen and displayed signs of cristae damage. Notably, frequent enlargement of the nuclear envelope space was reported, and distinctive compacted chromatin clusters were prominently observed (Fig. 1).

3.2. Quantitative assessment of cell damage using flow cytometry

To broaden the cohort of cells under investigation modelling the response to each experimental condition, and gain a quantitative understanding of the induced damages, we carried out a multiparametric flow cytometry analysis. As far as morphology is concerned, the direct detection of SSC and FSC allowed to discriminate different clusters of signals representing respectively the intact (A) and the damaged (B) cells. Concurrently, by incubating cells with a low concentration of PI,

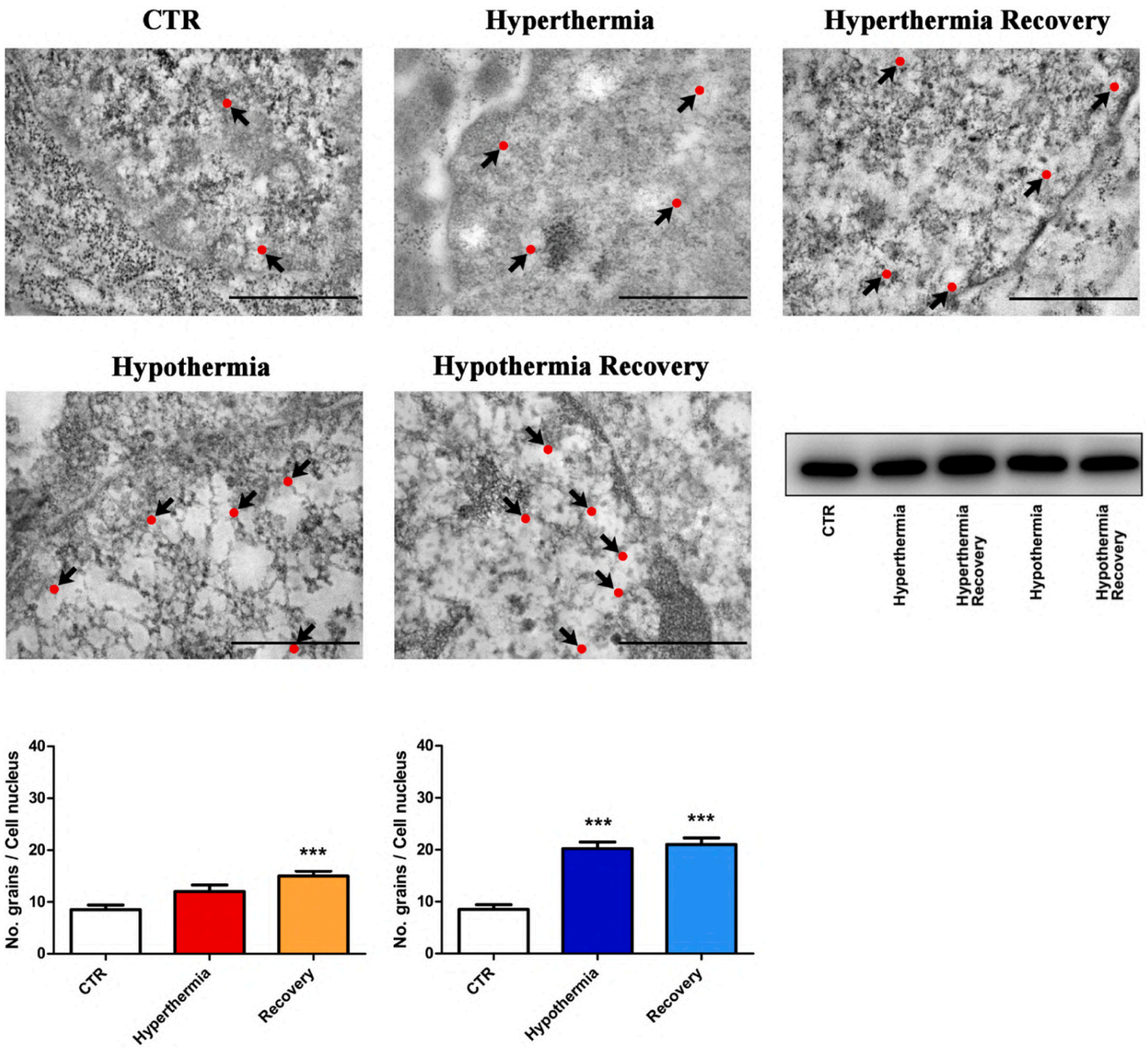

Fig. 5. H3K9Ac levels during thermal stresses. Immunolabelling (arrows) and western blotting show an increment in cells exposed to the thermal shocks, which is statistically relevant in the case of hypothermia and during both recoveries. A trend can also be visualized in the case of hyperthermia, although it is not statistically significant. Note the labelling locations in euchromatin and at the border of the condensed chromatin. Bars: 500 nm.

only damaged cells uptake the probe and exhibit a brilliant red fluorescent. Thus, the combination of SSC, FSC, and red fluorescence allowed to detect and quantitate the two subpopulations of interest. As expected, this investigation revealed an increase in the number of damaged cells under stress conditions compared to the control. In detail, the heat shock condition led to severe damages, accounting for 52.03% of the total sample measured, while the cold shock condition resulted in 41.20% damage, compared to the 15.22% of the controls. Notably, these parameters varied differently depending on the condition cells were recovering from. For instance, in cells recovering from the heat insult, the percentage of damaged cells is reduced to 29.79%, which represented an intermediate value between the control and the heat shock conditions. Remarkably, the number of damaged cells exiting from the cold shock and reverting to a normal temperature increased (45.58%). These findings collectively indicate the heat shock condition and the recovery from the cold shock to be the harshest phase (Fig. 2).

3.3. Histone PTMs under thermal stress

In light of the results observed in cell morphology and cell viability in the different conditions of thermal stresses, we investigated the distribution and abundance of histone PTMs in cells undergoing the thermal shocks. Specifically, we examined two transcription-silencing associated markers, trimethylated lysine 9 on histone H3 (H3K9me3) and trimethylated lysine 27 on histone H3 (H3K27me3). Immunogold labelling and western blotting revealed a statistically relevant increase in the abundance of H3K9me3 in cells subjected to hyperthermia and during recovery from hypothermia (Fig. 3). Similarly, H3K27me3 exhibited a noteworthy increment during heat shock and cold shock recovery (Fig. 4). Additionally, we assessed the levels of the transcription-instructive marker acetylated lysine 9 on histone H3 (H3K9Ac), which showed an increase during the stresses, particularly during hypothermia, and the recoveries (Fig. 5).

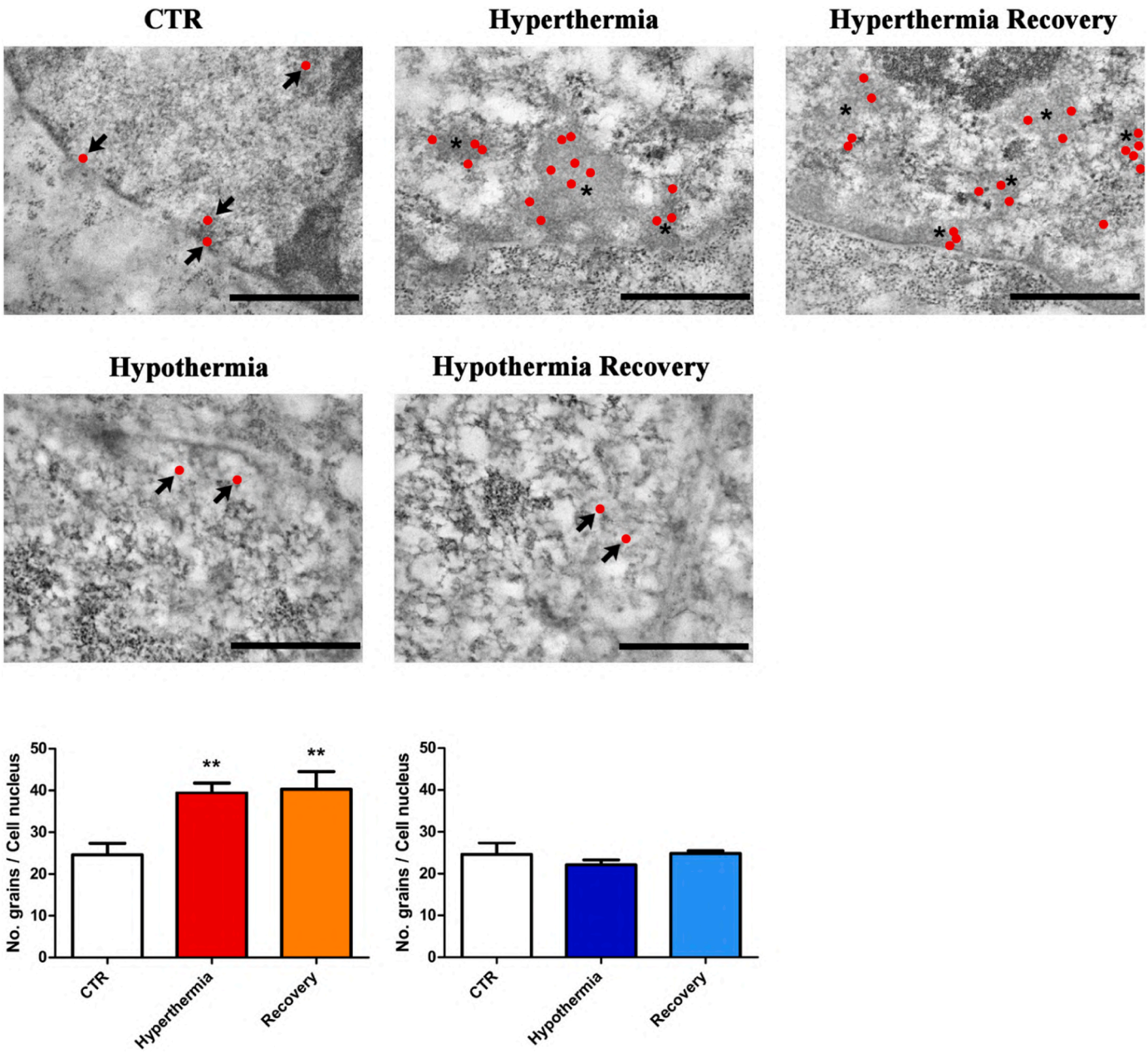

Fig. 6. 5mC levels during thermal stresses. Immunolabelling (arrows) reveals a statistically significant increase in 5mC abundance during heat shock and its recovery, while no significant differences are reported during the cold stress. Note the localization of 5mC labelling in condensed chromatin (asterisk) and its periphery. Bars: 500 nm.

3.4. DNA methylation and demethylation during thermal stress

Next, we directed our attention to DNA methylation and demethylation, in particular assessing 5mC and 5hmC levels, as well as the methylating and demethylating enzymes DNMT3a and TET2. Our analysis revealed a significant increase in 5mC abundance during heat shock and recovery from this insult. Interestingly, no significant alterations were highlighted during cold shock (Fig. 6). Consistently with these findings, we observed statistically relevant reductions in 5hmC levels during both thermal insults and their corresponding recoveries (Fig. 7).

According to the reported 5mC increase during heat shock, our investigations revealed an increment in the methylating enzymes DNMT3a during hyperthermia. Compared to the phase of acute thermal stress, we report a reduction during the recovery. Notably, the same outcome was verified for the hypothermic stress and its corresponding recovery (Fig. 8). Consistently with the decrease in 5hmC levels during the heat shock, we also observed a reduction in the levels of the demethylating enzyme TET2 during this type of stress. Interestingly, despite the highlighted reduction in 5hmC levels during the cold shock, we report a significant increment in TET2 abundance during cold shock, especially in its corresponding recovery (Fig. 9).

3.5. Impact of thermal stress on chromatin architecture

Having established alterations at the level of DNA and histone PTMs, we next explored the potential consequences on chromatin architecture. Confocal microscopy images of cells stained with Hoechst 33258 revealed a significant increase in chromatin compaction during the heat and cold shocks, with the formation of dense chromatin clusters as already described for electron microscopy. Interestingly, recoveries from thermal stresses are characterized by an intermediate level of

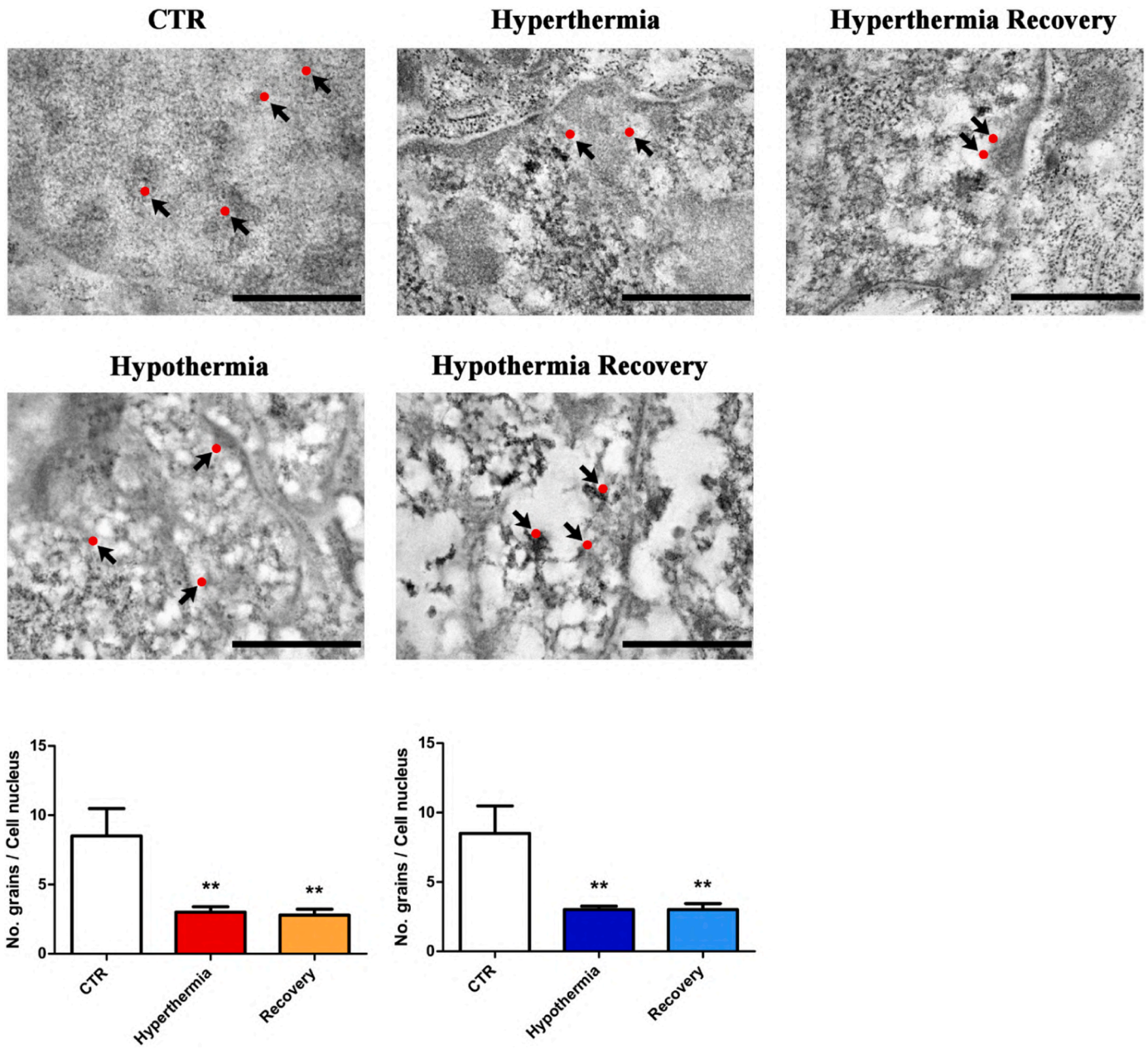

Fig. 7. 5hmC levels during thermal stresses. Immunolabelling (arrows) shows a significant decrease in this marker levels during all experimental conditions. Bars: 500 nm.

chromatin compaction between the controls and the stress conditions, suggesting a possible reversion for the surviving cells to the initial pre-stress conditions (Fig. 10).

3.6. Effect of thermal stress on EZH2 expression and location

Having established the impact of thermal stress on chromatin architecture, we decided to deepen our investigation focusing on EZH2 distribution and abundancy, the enzymatic catalytic subunit of the Polycomb repressive complex 2, whose activity is associated with chromatin remodeling via H3K27 trimethylation. STED imaging revealed that EZH2 localized in areas negative for the SPY-505 DNA signal with sub-diffraction limited resolution in individual nuclei. Statistical analysis conducted assessing the nuclear level of EZH2 highlights a reduction in its signal during hyperthermia, as well as during the recovery from hypothermia. Remarkably, western blot and qPCR analyses revealed no statistically significant alterations in the total EZH2 expression, suggesting a direction towards maintaining a comparable total amount of this enzyme throughout the stress conditions (Fig. 11).

4. Discussion

The present study aimed to investigate the effects of temperature shocks on chromatin architecture and epigenetic modifications in human cells. Hyperthermia is a well-studied form of stress, and it activates a common series of molecular pathways that are also triggered by various cell stressors, such as heavy metals, membrane perturbations, oxidative stress, and by multiple pathophysiological conditions (Dukay et al., 2019). Conversely, hypothermia has received less attention, but its clinical and commercial importance is increasingly recognized, with applications ranging from agriculture to therapeutics and pathology (Zhu, 2016; Xu et al., 2022). To conduct this investigation, HeLa cells were selected for their high proliferation and transcription rate, enabling rapid responses to the stressful conditions and expression of the

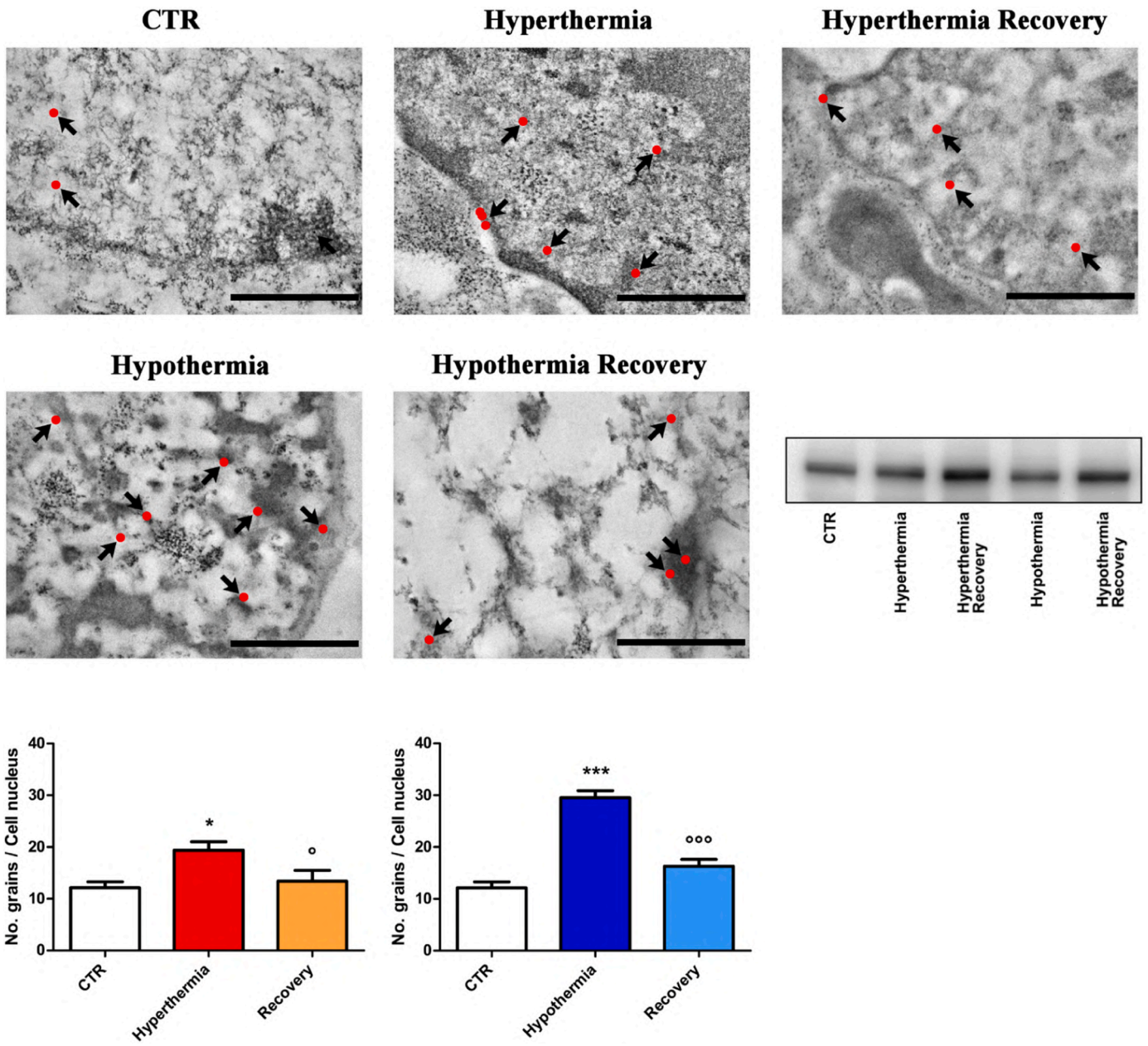

Fig. 8. DNTM3a levels during thermal stresses. Immunolabelling (arrows) and western blotting display statistically relevant increments during hyperthermia and hypothermia. Bars: 500 nm.

studied modifications. Temperatures were chosen to induce a consistent stress response and to allow the assessment of the investigated aspects in cells undergoing the stress, as well as in cells recovering at physiological temperatures following the transient heat and cold shocks.

Here, our data report temperature-dependent alterations in methylation patterns. Human cells subjected to heat shock displayed an increase in the epigenetic modifications associated with the silencing of gene expression. Indeed, we observed an increment in the level of DNA methylation in the form of 5mC, accompanied by a corresponding decrease in its transcription-promoting demethylation intermediate, 5hmC. Similarly, we found an increase in heterochromatin-associated histone PTMs such as H3K9me3 and H3K27me3. These findings agree with previous studies that highlighted how numerous genes undergo DNA methylation during hyperthermia (Xu et al., 2020). However, most of these recent findings are limited to non-human models. For instance, the study of Chang and colleagues highlights an increment in the methylation levels of the aquatic organism sea cucumber following heat stress (Chang et al., 2023). Liu and colleagues reached a similar result in the plant model *Saccharina japonica* (Liu et al., 2023). The existing studies conducted on human cells and tissues agree, to our knowledge, with our results. For instance, Bind and colleagues reported a temperature-dependent increase in CpG sites methylation in newborn placental samples and in the repeat element Alu of leukocytes (Bind et al., 2014).

Conversely, cold shock presented a more complex scenario, with 5mC levels remaining unaltered while showing a significant reduction of 5hmC labelling. Furthermore, we observed an increment in histone PTMs associated with both gene silencing and instructive for gene expression, especially during the recovery from the cold shock. The reduction in 5hmC levels and the increase in the heterochromatin-associated histone PTMs during hypothermia may be attributed to the global reduction in gene expression induced by this stress condition. Notably, the recovery from the cold shock proved to be an extremely harsh period for cells, as evidenced by ultrastructural analysis and flow

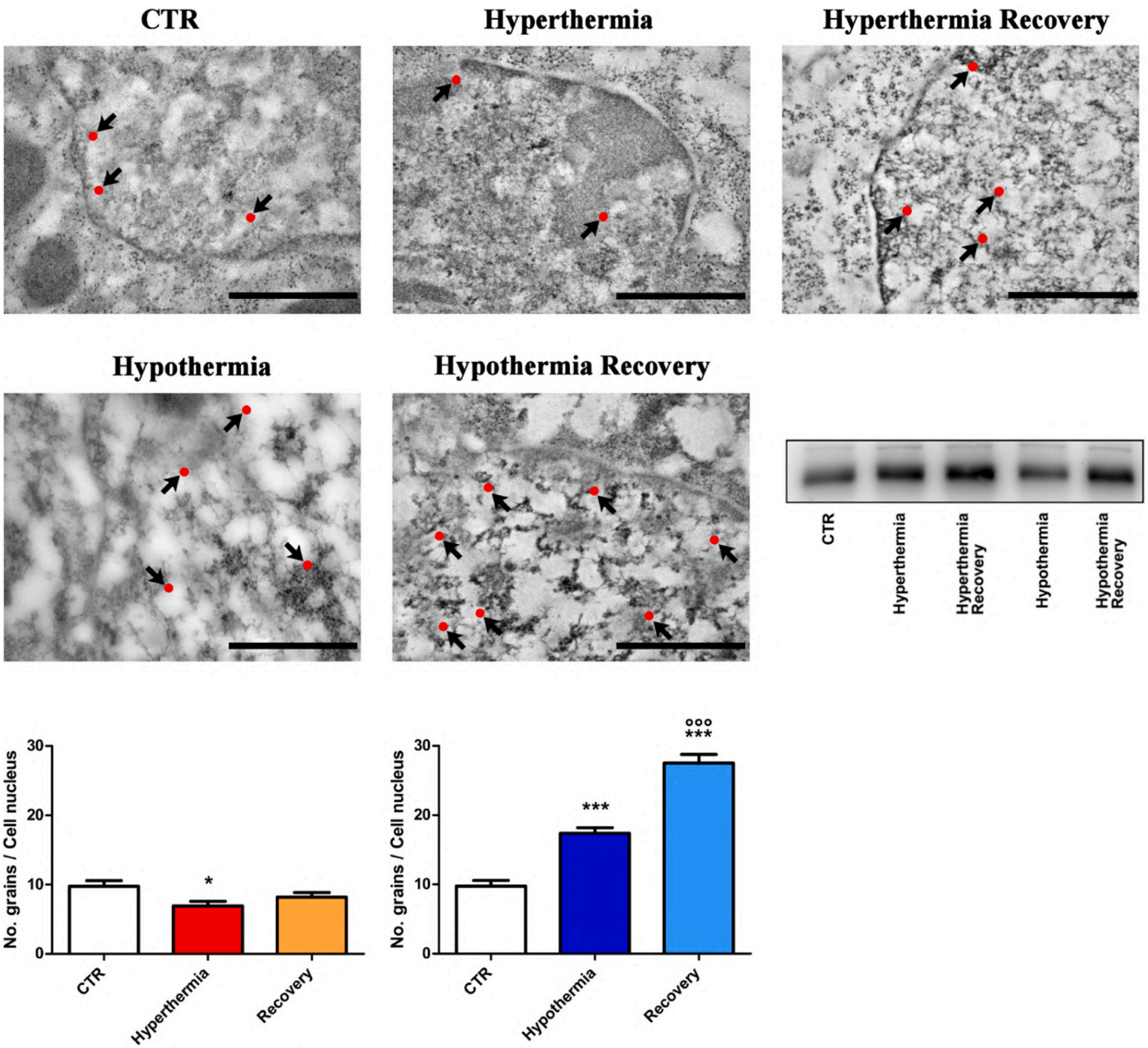

Fig. 9. TET2 levels during thermal stresses. Immunolabelling (arrows) and western blotting highlight a significant reduction during hypothermia, whereas a relevant increase is observed during hypothermia and its corresponding recovery. Bars: 500 nm.

cytometry. This suggests that successful recovery from such condition may require a highly dynamic, precise, and active regulation of gene expression and chromatin organization. Once again, most of the existing works are prevalently focused on plants. Nonetheless, similarly to our findings, the analysis conducted by Liu and colleagues highlighted a complex scenario with hypothermia-dependent increments in both methylation and demethylation (Liu et al., 2017) in *Brassica rapa*. Moreover, Araz and coworkers described cold-dependent increments in methylation levels in *Capsicum annuum L.* (Araz et al., 2022). Focusing on human samples, these outcomes are corroborated by other works, for instance, Lim and colleagues correlated low temperature with gene silencing via hypermethylation (Lim et al., 2017), while Zha and co-workers highlighted increments in histone acetylation in brown adipocytes following hypothermia (Zha et al., 2015).

It is worth noting that many investigations are based on Epigenome-Wide Association Study (EWAS) and Whole Genome Bisulfite Sequencing (WGBS) (Wei et al., 2021). However, approaches such as EWAS and WGBS and similar techniques share certain intrinsic set of limitations in their most widespread applications, ranging from low mapping efficiencies to limitation in the ethnicity of the EWAS subjects (Wei et al., 2021; Raine et al., 2022). Furthermore, genetic information is not arranged linearly; instead, its spatial configurations play a critical role in is at the base of gene accessibility for their transcription (Akdemir et al., 2020). Determination of chromatin organization hold a critical role in understanding all those mechanisms modulating the genome function (Zannino et al., 2021). In this context, to our knowledge, our study is among the firsts presenting correlations between temperature variations and epigenetic modification with a clear focus on chromatin architecture and its spatial organization, by means of ultrastructural and sub-diffraction limited super-resolution microscopy techniques.

5. Concluding remarks

During their existence, cells must cope with a series of alterations in

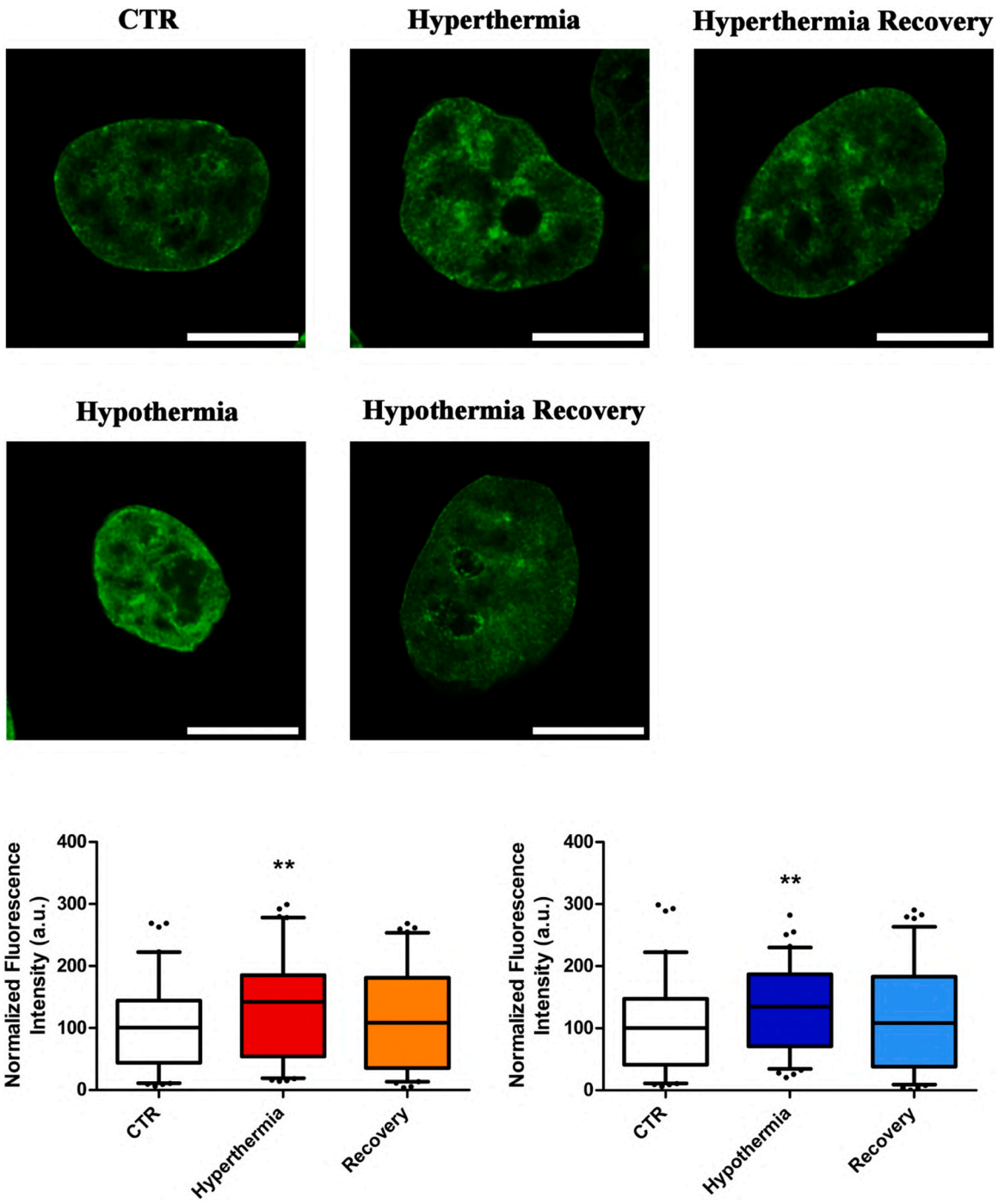

Fig. 10. Chromatin compaction level during thermal stresses. Confocal images revealed increase in chromatin condensation during both hyperthermia and hypothermia. At least a partial reversion to the pre-stress situation is highlighted if cells are given time to recover. Bars: 10 μm.

their environment. Several forms of cell insults, such as temperature variations, exposure to toxic substances or heavy metals, and alterations in osmolarity or redox state, directly trigger alterations in the epigenetic state (Casali et al., 2022a). Temperature alterations are among the most common form of cell stress; however, evidence about their impact on human epigenetics remains scarce. For instance, DNA methylation and demethylation are frequently observed to be deregulated in various cancer types, due to their importance in gene expression regulation (Shi et al., 2021). One of the main limitations of current works relies in the fact that epigenetic profiles in surrogate tissues may not actually reflect the epigenetic state in a target organ or organism, requiring extreme carefulness when interpreting results (Xu et al., 2020). More studies are needed to expand the current knowledge, and only the combination of different approaches into a coherent model of analysis may allow for a broader understanding of the cell stress-gene expression relationship, facilitating advances in health and commercial sectors.

Funding

This research was funded by the Italian Ministry of Education, University and Research (MIUR): Dipartimenti di Eccellenza Program (2018-2022) — Department of Biology and Biotechnology "L. Spallanzani", University of Pavia (to M.B.).

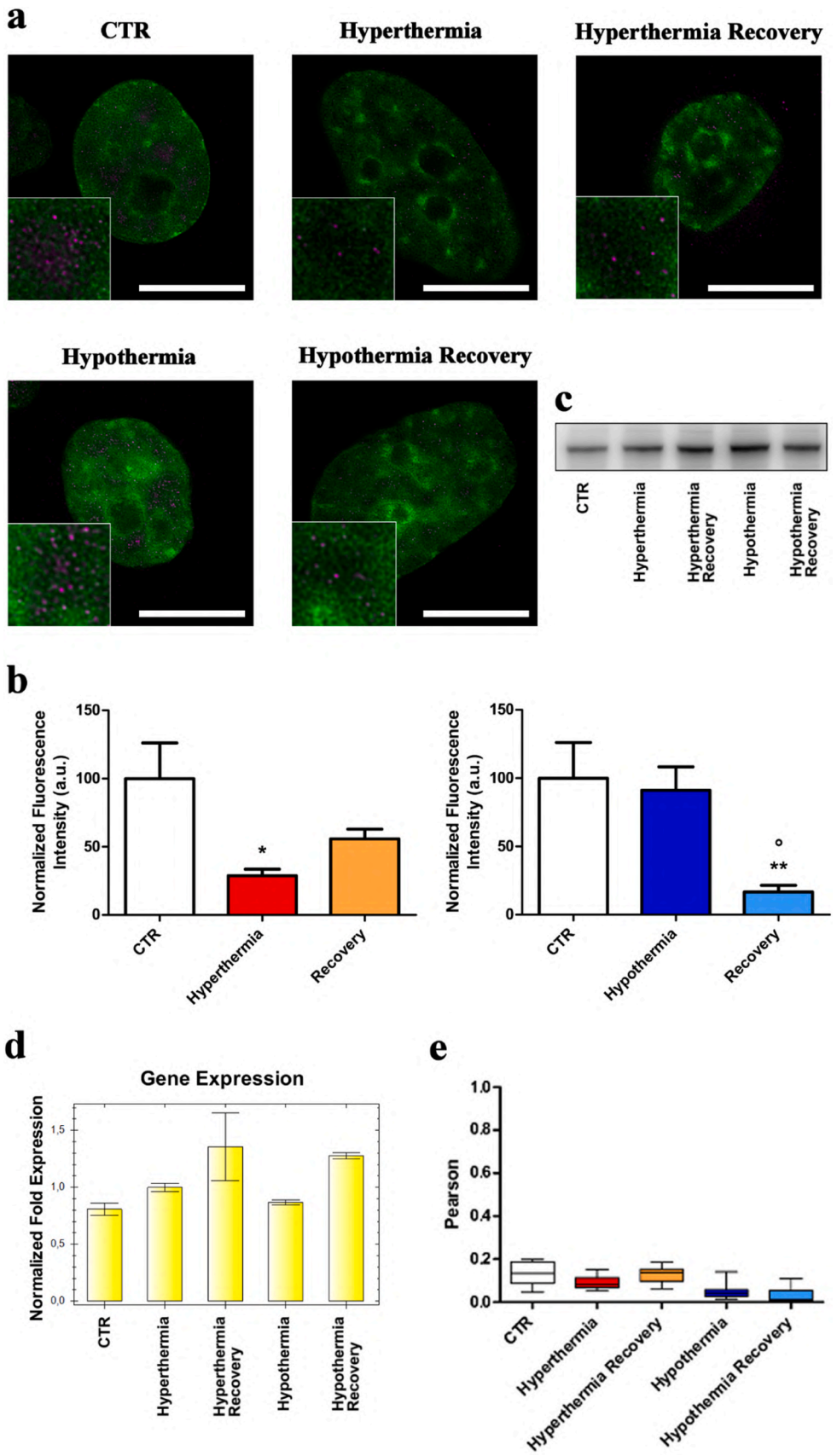

Fig. 11. STED super-resolution imaging of EZH2 (magenta) and DNA (green) during thermal stresses. **a,b** Immunofluorescence highlighted that during hyperthermia and recovery from hypothermia, EZH2 nuclear levels are significantly reduced. c,**d** Western blotting and qPCR showed no statistically relevant variations in the total expression levels of EZH2. **e** Pearson correlation coefficient revealed EZH2 preferential spatial location in SPY505-DNA negative areas. Bars: 10 μm.

CRediT authorship contribution statement

Claudio Casali: Conceptualization, Methodology, Validation, Formal analysis, Investigation, Data curation, Writing – original draft, Writing – review & editing, Visualization, Project administration. **Luca Galgano:** Validation, Formal analysis, Investigation, Data curation. **Lorena Zannino:** Validation, Formal analysis, Investigation, Data curation. **Stella Siciliani:** Validation, Formal analysis, Investigation, Data curation. **Margherita Cavallo:** Validation, Formal analysis, Investigation, Data curation. **Giuliano Mazzini:** Methodology, Investigation, Resources, Data curation, Writing – review & editing, Supervision. **Marco Biggiogera:** Methodology, Resources, Writing – review & editing, Supervision, Project administration, Funding acquisition.

Declaration of Competing Interest

The authors declare that they have no known competing financial interests or personal relationships that could have appeared to influence the work reported in this paper.

Data Availability

Data will be made available on request.

Acknowledgements

Authors express their gratitude to Gloria Milanesi and Paola Veneroni (Department of Biology and Biotechnology, University of Pavia). Authors also sincerely thank Massimo Boiocchi and Amanda Oldani (Centro Grandi Strumenti, PASS-BioMed Imaging).

Appendix A. Supporting information

Supplementary data associated with this article can be found in the online version at doi:10.1016/j.ejcb.2023.151373.

References

Abildgaard, A.B., Voutsinos, V., Petersen, S.D., Larsen, F.B., Kampmeyer, C., Johansson, K.E., Stein, A., Ravid, T., Andréasson, C., Jensen, M.K., Lindorff-Larsen, K., Hartmann-Petersen, R., 2023. HSP70-binding motifs function as protein quality control degrons. Cell Mol. Life Sci. 80, 32 https://doi.org/10.1007/s00018-022-04679-3.

Akdemir, K.C., Le, V.T., Kim, J.M., Killcoyne, S., King, D.A., Lin, Y.-P., Tian, Y., Inoue, A., Amin, S.B., Robinson, F.S., Nimmakayalu, M., Herrera, R.E., Lynn, E.J., Chan, K., Seth, S., Klimczak, L.J., Gerstung, M., Gordenin, D.A., O'Brien, J., Li, L., Deribe, Y.L., Verhaak, R.G., Campbell, P.J., Fitzgerald, R., Morrison, A.J., Dixon, J.R., Andrew Futreal, P., 2020. Somatic mutation distributions in cancer genomes vary with three-dimensional chromatin structure. Nat. Genet 52, 1178–1188. https://doi.org/10.1038/s41588-020-0708-0.

Araz, O., Ekinci, M., Yuce, M., Shams, M., Agar, G., Yildirim, E., 2022. Low-temperature modified DNA methylation level, genome template stability, enzyme activity, and proline content in pepper (Capsicum annuum L.) genotypes. Sci. Hortic. 294, 110761 https://doi.org/10.1016/j.scienta.2021.110761.

Aricthota, S., Rana, P.P., Haldar, D., 2022. Histone acetylation dynamics in repair of DNA double-strand breaks. Front. Genet 13, 926577. https://doi.org/10.3389/fgene.2022.926577.

Azarm, K., Smith, S., 2020. Nuclear PARPs and genome integrity. Genes Dev. 34, 285–301. https://doi.org/10.1101/gad.334730.119.

Bernhard, W., 1969. A new staining procedure for electron microscopical cytology. J. Ultra Res 27, 250–265. https://doi.org/10.1016/s0022-5320(69)80016-x.

Bind, M.-A., Zanobetti, A., Gasparrini, A., Peters, A., Coull, B., Baccarelli, A., Tarantini, L., Koutrakis, P., Vokonas, P., Schwartz, J., 2014. Effects of temperature and relative humidity on DNA methylation. Epidemiology 25, 561–569. https://doi.org/10.1097/EDE.0000000000000120.

Binder, M., Carr, R.M., Lasho, T.L., Finke, C.M., Mangaonkar, A.A., Pin, C.L., Berger, K. R., Mazzone, A., Potluri, S., Ordog, T., Robertson, K.D., Marks, D.L., Fernandez-Zapico, M.E., Gaspar-Maia, A., Patnaik, M.M., 2022. Oncogenic gene expression and epigenetic remodeling of cis-regulatory elements in ASXL1-mutant chronic myelomonocytic leukemia. Nat. Commun. 13, 1434 https://doi.org/10.1038/s41467-022-29142-6.

Buzzella, A., Mazzini, G., Vicini, R., Angelinetta, C., Pastoris, O., 2019. A preliminary study of an alternative method for evaluating skin sensitizing potential of chemicals. Int J. Cosmet. Sci. 41, 257–264. https://doi.org/10.1111/ics.12530.

Casali, C., Siciliani, S., Galgano, L., Biggiogera, M., 2022a. Oxidative stress and nuclear reprogramming: a pilot study of the effects of reactive oxygen species on architectural and epigenetic landscapes. Int. J. Mol. Sci. 24, 153. https://doi.org/10.3390/ijms24010153.

Casali, C., Siciliani, S., Zannino, L., Biggiogera, M., 2022b. Histochemistry for nucleic acid research: 60 years in the European Journal of Histochemistry. Eur. J. Histochem 66. https://doi.org/10.4081/ejh.2022.3409.

Cavalli, G., Heard, E., 2019. Advances in epigenetics link genetics to the environment and disease. Nature 571, 489–499. https://doi.org/10.1038/s41586-019-1411-0.

Chang, M., Ge, J., Liao, M., Rong, X., Wang, Y., Li, B., Li, X., Wang, J., Zhang, Z., Yu, Y., Wang, C., 2023. Genome-wide DNA methylation and transcription analysis reveal the potential epigenetic mechanism of heat stress response in the sea cucumber Apostichopus japonicus. Front. Mar. Sci. 10.

Collins, B.E., Greer, C.B., Coleman, B.C., Sweatt, J.D., 2019. Histone H3 lysine K4 methylation and its role in learning and memory. Epigenetics Chromatin 12, 7. https://doi.org/10.1186/s13072-018-0251-8.

Dukay, B., Csoboz, B., Tóth, M.E., 2019. Heat-shock proteins in neuroinflammation. Front. Pharm. 10, 920 https://doi.org/10.3389/fphar.2019.00920.

Greenberg, M.V.C., Bourc'his, D., 2019. The diverse roles of DNA methylation in mammalian development and disease. Nat. Rev. Mol. Cell Biol. 20, 590–607. https://doi.org/10.1038/s41580-019-0159-6.

He, B., Zhang, C., Zhang, X., Fan, Y., Zeng, H., Liu, J., Meng, H., Bai, D., Peng, J., Zhang, Q., Tao, W., Yi, C., 2021. Tissue-specific 5-hydroxymethylcytosine landscape of the human genome. Nat. Commun. 12, 4249 https://doi.org/10.1038/s41467-021-24425-w.

Hoboth, P., Sztacho, M., Quaas, A., Akgül, B., Hozák, P., 2023. Quantitative super-resolution microscopy reveals the differences in the nanoscale distribution of nuclear phosphatidylinositol 4,5-bisphosphate in human healthy skin and skin warts. Front. Cell Dev. Biol. 11, 1217637 https://doi.org/10.3389/fcell.2023.1217637.

Huang, H.-T., Figueroa, M.E., 2021. Epigenetic deregulation in myeloid malignancies. Blood 138, 613–624. https://doi.org/10.1182/blood.2019004262.

Joshi, K., Liu, S., Breslin S J, P., Zhang, J., 2022. Mechanisms that regulate the activities of TET proteins. Cell Mol. Life Sci. 79, 363 https://doi.org/10.1007/s00018-022-04396-x.

Lam, U.T.F., Chen, E.S., 2022. Molecular mechanisms in governing genomic stability and tumor suppression by the SETD2 H3K36 methyltransferase. Int. J. Biochem. Cell Biol. 144, 106155 https://doi.org/10.1016/j.biocel.2021.106155.

Li, N., Meng, G., Yang, C., Li, H., Liu, L., Wu, Y., Liu, B., 2022. Changes in epigenetic information during the occurrence and development of gastric cancer. Int. J. Biochem. Cell Biol. 153, 106315 https://doi.org/10.1016/j.biocel.2022.106315.

Li, X., Li, X.D., 2021. Integrative chemical biology approaches to deciphering the histone code: a problem-driven journey. Acc. Chem. Res. 54, 3734–3747. https://doi.org/10.1021/acs.accounts.1c00463.

Lim, Y.-H., Han, C., Bae, S., Hong, Y.-C., 2017. Modulation of blood pressure in response to low ambient temperature: the role of DNA methylation of zinc finger genes. Environ. Res. 153, 106–111. https://doi.org/10.1016/j.envres.2016.11.019.

Liu, A.Y., Bian, H., Huang, L.E., Lee, Y.K., 1994. Transient cold shock induces the heat shock response upon recovery at 37 degrees C in human cells. J. Biol. Chem. 269, 14768–14775.

Liu, F., Zhang, P., Liang, Z., Yuan, Y., Liu, Y., Wu, Y., 2023. The global dynamic of DNA methylation in response to heat stress revealed epigenetic mechanism of heat acclimation in Saccharina japonica. J. Phycol. 59, 249–263. https://doi.org/10.1111/jpy.13305.

Liu, T., Li, Y., Duan, W., Huang, F., Hou, X., 2017. Cold acclimation alters DNA methylation patterns and confers tolerance to heat and increases growth rate in Brassica rapa. J. Exp. Bot. 68, 1213–1224. https://doi.org/10.1093/jxb/erw496.

Livernois, A.M., Mallard, B.A., Cartwright, S.L., Cánovas, A., 2021. Heat stress and immune response phenotype affect DNA methylation in blood mononuclear cells from Holstein dairy cows. Sci. Rep. 11, 11371 https://doi.org/10.1038/s41598-021-89951-5.

Mazzini, G., Danova, M., 2017. Fluorochromes for DNA staining and quantitation. Methods Mol. Biol. 1560, 239–259. https://doi.org/10.1007/978-1-4939-6788-9_18.

McCaw, B.A., Stevenson, T.J., Lancaster, L.T., 2020. Epigenetic responses to temperature and climate. Integr. Comp. Biol. 60, 1469–1480. https://doi.org/10.1093/icb/icaa049.

Metzger, D.C.H., Schulte, P.M., 2017. Persistent and plastic effects of temperature on DNA methylation across the genome of threespine stickleback (Gasterosteus aculeatus). Proc. Biol. Sci. 284, 20171667. https://doi.org/10.1098/rspb.2017.1667.

Parreno, V., Martinez, A.-M., Cavalli, G., 2022. Mechanisms of Polycomb group protein function in cancer. Cell Res. 32, 231–253. https://doi.org/10.1038/s41422-021-00606-6.

Raftery, A.E., Zimmer, A., Frierson, D.M.W., Startz, R., Liu, P., 2017. Less Than 2 °C Warming by 2100 Unlikely. Nat. Clim. Chang 7, 637–641. https://doi.org/10.1038/nclimate3352.

Raine, A., Lundmark, A., Annett, A., Wiman, A.-C., Cavalli, M., Wadelius, C., Bergin, C., Nordlund, J., 2022. scSPLAT, a scalable plate-based protocol for single cell WGBS library preparation. Sci. Rep. 12, 5772 https://doi.org/10.1038/s41598-022-09798-2.

Reynolds, E.S., 1963. The use of lead citrate at high pH as an electron-opaque stain in electron microscopy. J. Cell Biol. 17, 208–212. https://doi.org/10.1083/jcb.17.1.208.

Rueden, C.T., Schindelin, J., Hiner, M.C., DeZonia, B.E., Walter, A.E., Arena, E.T., Eliceiri, K.W., 2017. ImageJ2: ImageJ for the next generation of scientific image data. BMC Bioinforma. 18, 529 https://doi.org/10.1186/s12859-017-1934-z.

Santiago, M., Antunes, C., Guedes, M., Iacovino, M., Kyba, M., Reik, W., Sousa, N., Pinto, L., Branco, M.R., Marques, C.J., 2020. Tet3 regulates cellular identity and DNA methylation in neural progenitor cells. Cell Mol. Life Sci. 77, 2871–2883. https://doi.org/10.1007/s00018-019-03335-7.

Schindelin, J., Arganda-Carreras, I., Frise, E., Kaynig, V., Longair, M., Pietzsch, T., Preibisch, S., Rueden, C., Saalfeld, S., Schmid, B., Tinevez, J.-Y., White, D.J., Hartenstein, V., Eliceiri, K., Tomancak, P., Cardona, A., 2012. Fiji - an Open Source platform for biological image analysis. Nat. Methods 9, 10. https://doi.org/10.1038/nmeth.2019.

Sharma, M., Tollefsbol, T.O., 2022. Combinatorial epigenetic mechanisms of sulforaphane, genistein and sodium butyrate in breast cancer inhibition. Exp. Cell Res. 416, 113160 https://doi.org/10.1016/j.yexcr.2022.113160.

Shi, J., Xu, J., Chen, Y.E., Li, J.S., Cui, Y., Shen, L., Li, J.J., Li, W., 2021. The concurrence of DNA methylation and demethylation is associated with transcription regulation. Nat. Commun. 12, 5285 https://doi.org/10.1038/s41467-021-25521-7.

Turpin, M., Salbert, G., 2022. 5-methylcytosine turnover: mechanisms and therapeutic implications in cancer. Front. Mol. Biosci. 9.

Tyagi, S.C., Stanisic, D., Singh, M., 2021. Epigenetic memory: gene writer, eraser and homocysteine. Mol. Cell Biochem 476, 507–512. https://doi.org/10.1007/s11010-020-03895-4.

Wang, L., You, X., Ruan, D., Shao, R., Dai, H.-Q., Shen, W., Xu, G.-L., Liu, W., Zou, W., 2022. TET enzymes regulate skeletal development through increasing chromatin accessibility of RUNX2 target genes. Nat. Commun. 13, 4709 https://doi.org/10.1038/s41467-022-32138-x.

Wei, S., Tao, J., Xu, J., Chen, X., Wang, Z., Zhang, N., Zuo, L., Jia, Z., Chen, H., Sun, H., Yan, Y., Zhang, M., Lv, H., Kong, F., Duan, L., Ma, Y., Liao, M., Xu, L., Feng, R., Liu, G., Project, T.E., Jiang, Y., 2021. Ten Years of EWAS. Adv. Sci. 8, e2100727 https://doi.org/10.1002/advs.202100727.

Wu, J., Zhang, W., Li, C., 2020. Recent advances in genetic and epigenetic modulation of animal exposure to high temperature. Front Genet 11, 653. https://doi.org/10.3389/fgene.2020.00653.

Xie, L., Liu, Z., 2021. Single-cell imaging of genome organization and dynamics. Mol. Syst. Biol. 17, e9653 https://doi.org/10.15252/msb.20209653.

Xu, G., Li, T., Huang, Y., 2022. The effects of intraoperative hypothermia on postoperative cognitive function in the rat hippocampus and its possible mechanisms. Brain Sci. 12, 96. https://doi.org/10.3390/brainsci12010096.

Xu, R., Li, Shuai, Guo, S., Zhao, Q., Abramson, M.J., Li, Shanshan, Guo, Y., 2020. Environmental temperature and human epigenetic modifications: a systematic review. Environ. Pollut. 259, 113840 https://doi.org/10.1016/j.envpol.2019.113840.

Yang, C.-X., Chen, L., Mou, Q., Yang, Y.-W., Wang, Y., Yin, Z., Du, Z.-Q., 2022. HSP90AA1 promotes viability and lactate production but inhibits hormone secretion of porcine immature Sertoli cells. Theriogenology 194, 64–74. https://doi.org/10.1016/j.theriogenology.2022.09.027.

Zannino, L., Casali, C., Siciliani, S., Biggiogera, M., 2021. The dynamics of the nuclear environment and their impact on gene function. J. Biochem 169, 259–264. https://doi.org/10.1093/jb/mvaa091.

Zha, L., Li, F., Wu, R., Artinian, L., Rehder, V., Yu, L., Liang, H., Xue, B., Shi, H., 2015. The histone demethylase UTX promotes brown adipocyte thermogenic program via coordinated regulation of H3K27 demethylation and acetylation. J. Biol. Chem. 290, 25151–25163. https://doi.org/10.1074/jbc.M115.662650.

Zhu, J., Cao, X., Deng, X., 2023. Epigenetic and transcription factors synergistically promote the high temperature response in plants. Trends Biochem Sci. S0968-0004 (23), 00140–00148. https://doi.org/10.1016/j.tibs.2023.06.001.

Zhu, J.-K., 2016. Abiotic stress signaling and responses in plants. Cell 167, 313–324. https://doi.org/10.1016/j.cell.2016.08.029.